Biophysical Chemistry 250 (2019) 106174

Contents lists available at ScienceDirect

Biophysical Chemistry

journal homepage: www.elsevier.com/locate/biophyschem

Delineating the effect of mutations on the conformational dynamics of N-terminal domain of TDP-43

Vijay Kumar[a,*], Preeti Pandey[b], Danish Idrees[c], Amresh Prakash[b,*], Andrew.M. Lynn[b]

[a] Amity Institute of Neuropsychology & Neurosciences, Amity University, Noida, UP 201301, India
[b] School of Computational & Integrative Sciences, Jawaharlal Nehru University, New Delhi 110067, India
[c] School of Life Sciences, Jawaharlal Nehru University, New Delhi 110067, India

HIGHLIGHTS

- All atom MD simulation of NTD variants at 300 K
- Mutations in NTD affect its stability, dynamics and function.
- Leu28Ala mutation strictly destabilized the NTD.
- Loss of β strands upon mutation leads to the structural destabilization of NTD.
- Mutations lead to the structural instability, the reduced intramolecular interactions and the early unfolding of NTD protein.

GRAPHICAL ABSTRACT

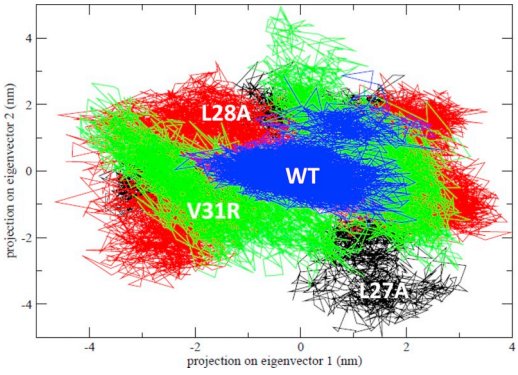

ARTICLE INFO

Keywords:
NTD
Mutations
Molecular dynamics simulation
Stability
Flexibility
Intermolecular interactions
Dysfunction

ABSTRACT

The structural integrity of N-terminal domain (NTD) of TAR DNA-binding protein-43 (TDP-43) is essential for the biological functions of TDP-43 involved in neurodegenerative diseases. Here, we used all-atom molecular dynamics (MD) simulations to understand the folding, dynamics and conformational stability of four variants of NTD, the wild type (WT) and three mutants (L27A, L28A and V31R). The deleterious and destabilizing nature of NTD mutants were predicted on DynaMut and SAAFEC server. Results show that predicted mutations modulate the conformational stability and flexibility of NTD. The effect of mutations on the conformational dynamics of NTD was studied through the free-energy landscape (FEL), essential dynamics (ED), hydrogen-bonds and intermolecular contact map. We observed that the mutations disrupt the intermolecular interactions between the dimeric NTD besides affecting the long-range intramolecular contacts, resulting in a less compact structure. ED essentially provides the collective motion of protein and we observed that the mutation increased the overall motions of the protein which might result in protein dysfunction. FEL shows the different conformational transitions of WT and mutants which revealed the structural basis of protein destabilization and unfolding due to mutation. We find that L28A has most of the deleterious effect compared to other two mutations, L27A and V31R. These results obtained here are well correlated with reported experimental studies which show the disruption of protein folding, stability and function with these mutations. Hence this computational study describes

* Corresponding authors.
E-mail addresses: vkumar33@amity.edu (V. Kumar), amreshprakash@jnu.ac.in (A. Prakash).

https://doi.org/10.1016/j.bpc.2019.106174
Received 28 December 2018; Received in revised form 6 March 2019; Accepted 21 April 2019
Available online 22 April 2019

the structural details to unravel the mutant effects at the atomistic resolution and has implications for understanding the TDP-43's physiological and pathological role.

1. Introduction

Aberrant aggregates of Tar DNA-Binding Protein of 43 kDa (TDP-43) have been described in patients with Amyotrophic Lateral Sclerosis (ALS), frontotemporal lobar degeneration (FTLD) [1–3] and more recently in patients with Alzheimer's, Parkinson's and Huntington's diseases [4–6]. TDP-43 is a versatile RNA-binding protein involved in cellular process such as RNA-metabolism (transcription, translation, miRNA processing, mRNA transport across nucleus) [7–9], apoptosis [10], cell division [11], embryo development [12], and stress response [13]. Key to these functions are TDP-43's two stable folded RNA recognition motifs (RRM) domains. TDP-43 has a glycine-rich, disordered C-terminal domain (CTD) which contains almost all the pathologically linked ALS-mutations [14] and has high propensity to self-assemble [15,16], phase separate [17,18], and aggregate [1].

TDP-43 also contains an N-terminal domain (NTD) whose structure and structural integrity is essential for biological functions of TDP-43. Structurally, the NTD consist of five β-strands (β2-β1-β5-β3-β4) packed against one α-helix and an additional β-hairpin which is present in the loop between β4 and β5, representing the domain architecture of NTD as reminiscent of Ubiquitin and DIX domains [19].

Interestingly, a dichotomy in TDP-43 has been mentioned, where NTD is involved both in physiological and pathological functions of TDP-43 [20–24]. Therefore, the folding dynamics and conformational stability studies of NTD is essential to underpinning the mechanisms behind the dichotomy of TDP-43. Tsoi et al. [25] showed that low pH induces the destabilization and unfolding of the NTD with the presence of multiple native thermodynamic states. We have recently performed all-atom MD simulations of NTD in 8 M urea at 300 K–500 K and reported that unfolding of the NTD proceeds through various stable and meta-stable intermediate states [26].

Mompean et al. [27] studied the folding and functions of NTD and NTD mutations like Leu27Ala (L27A), Leu28Ala (L28A) and Val31Arg (V31R) and showed that L27A disrupts the dimerization of NTD without being unfolded whereas, L28A severely destabilized the NTD and remain unfolded. The V31R mutation abolished TDP-43 splicing functions and promotes aggregation by disrupting the hydrophobic core and subsequently unfolding the NTD. Their study suggests that the NTD must be stably folded for TDP-43 to be able to carry out its physiological functions.

In this regard, a mechanistic study based on structural and dynamics analysis of the NTD variants will be beneficial to understand the folding and functions of NTD. Here, we computationally investigated the conformational stability, folding and dynamics of the four NTD variants namely, wild type NTD, L27A, L28A and V31R and provide the mechanisms leading to the destabilization and dysfunction of mutant NTD. This study will further increase our understanding toward the folding, stability and dynamics of NTD in integration of TDP-43 physiological and pathological functions, which is implicated in neurodegenerative diseases.

2. Materials and methods

2.1. Predicting the mutational effects on NTD stability, folding and function

The change in dynamics and stability of NTD upon mutation was predicted via the DynaMut server which incorporates the dynamics component to mutation analysis. DynaMut implements normal mode analysis (NMA) through two different tools, Bio3D [28] and ENCoM [29] and analyze the impact of mutation on protein dynamics and stability resulting from vibrational entropy changes. DynaMut also includes other well-established structural methods mCSM [30], SDM [31], and the consensus method DUET [32] to provide accurate assessment of the change in protein stability due to mutation. The output is represented in terms of the predicted change in stability (in kcal/mol) as well as the variation in entropy energy between wild-type and mutant structures (in kcal/mol/K).

Further, we predicted mutation induced change of the protein folding free energy by the SAAFEC (Single Amino Acid Folding free Energy Changes) server [33]. The server utilizes a knowledge-based Molecular Mechanics Poisson– Boltzmann (MM/PBSA) and a statistical description of the biophysical features of proteins to compute the folding free energy change induced by mutation. Finally, the webserver PREDICT-SNP [34] predicted the mutation induced change in protein functions. This tool employs a consensus of six different predictors (SIFT, SNAP, PhD-SNP, PolyPhen-1, PolyPhen-2 and MAPP) along with a confidence score of the predictions.

2.2. MD simulation

All atoms MD simulations were carried to examine the conformational dynamics of N-terminal domain of TDP-43 (PDB ID: 5MDI) and its mutants (L27A, L28A and V31R). The structure of the mutants was generated and optimized using the molecular modeling tool, Chimera (https://www.cgl.ucsf.edu/chimera/). All the simulations were performed using the Gromacs package v5.1.4 and CHARMM27 force field at temperature 300 K [35]. The water model TIP3P was used to the protein and Na^+ and Cl^- ions (0.15 M) were added to neutralize the system. The energy minimization process involves 5000 steps of each, steepest descent followed by conjugant gradients. Further, each system was equilibrated for 1 ns with two ensemble process NVT and NPT, and the periodic boundary condition (PBC) was applied to x-, y- and z directions. The temperature was kept constant using Berendsen thermostat [36] and the pressure (1 bar) was maintained by Parrinello-Rahman pressure coupling [37]. The algorithm, LINC was used to constrain the bonds [38] and the long-range electrostatic interactions were handled with the method, particle mesh Ewald (PME) [39]. Lennard- Jones potential has cutoff of radius 1.2 nm and was utilized for calculation of van der Waals interactions. Finally, the NPT ensemble was used to perform production run for 250 ns and the trajectory was recorded at the time interval of 5 ps. All the calculations were done on the machine Intel i7-x86–64 CPU compatible with OS Centos 7 and CUDA enabled NVIDIA graphics processing units (GPUs) [40].

2.3. MD trajectory analysis

The conformational order parameters, RMSD (root mean square deviation), R_g (radius of gyration) and SASA (solvent accessible surface area) were analyzed using the Gromacs utilities and python scripts with MDTraj [41]. DSSP was used to track the evolution of secondary structures during the simulation [43].

2.4. Free energy landscape (FEL)

The free-energy landscape (FEL) as function of reaction coordinates (P), R_g and the fraction of the native contacts (Nc) was generated by the Boltzmann inversion ($F = -RT \ln P$) [44,45]. The native contacts were defined as the minimal contacts between the pairs of heavy atoms ≤ 0.4 nm [46]. We also constructed an additional FEL as a function of RMSD-Nc for validating the ensemble obtained.

2.5. Principal component analysis (PCA)

The correlated motion is a central characteristic of the macromolecules and defines the function. Principal Component Analysis (PCA) method was used to define the correlated motion of the macromolecules [47–49]. This method involves the calculation from the covariance matrix, C and is calculated by the equation as:

$$C = \langle (x(t) - \langle x \rangle)(x(t) - \langle x \rangle)^T \rangle \quad (1)$$

where, the coordinates at time 't' is represented as x (t), the mean position denoted by < x > and < > represents the average of the ensembles. The covariance matrix C is then diagonalized to give the set of eigenvalues and eigenvectors.

$$C = T \Lambda T^T \quad (2)$$

where, Λ is the diagonalized matrix of eigenvalues and T contains the eigenvectors.

3. Results and discussion

Mutations alter the protein folding, dynamics, stability and its function often resulting in pathological consequences [50–52]. In this study, we provide insights toward the effects of point mutations, L27A, L28A, and V31R on the folding, dynamics and stability of NTD which is responsible for physiological oligomerization and pathological aggregation of TDP-43. Additionally, how these mutants alter the NTD conformations and the dimeric interface were elucidated in this study.

3.1. Effects of the mutation on the dynamics, stability, folding and function on the NTD

To study the mutation induced changes in structural stability of NTD, we utilized DynaMut webserver that predict the change in the dynamics and stability of a protein triggered by mutation. DynaMut predicted that all three mutations significantly destabilized the protein with the maximum destabilizing effect was shown by L28A (Table 1). In addition, DynaMut server also predicted the increase in vibrational entropy (i.e. molecular flexibility) for L27A and L28A, suggesting the increase in dynamics for these two mutations. These predictions results are in agreement with previous experimental study also [27].

In addition, the results at SAAFEC webserver also predicted that the mutation L28A significantly altered the folding, solvation, entropy and electrostatic energy of NTD (Table 2). Thus, the mutation L28A and L27A damages the structural stability and dynamics of the protein. Further, the effect of mutation on the function of protein was predicted using the PREDICT-SNP tool, which shows a consensus result of the six predictors and combines the results with the confidence scores. All the three mutations were predicted to be deleterious from five out of six predictors, suggesting the deleterious effect of mutants, L27A, L28A and V31R on NTD, with a high confidence score of 0.75, 0.79 and 0.71, respectively (Table 3).

Overall, the prediction results suggest that the mutations significantly impaired the protein folding, dynamics, stability and function. This impact of mutation on protein was further studied using MD simulations to understand its influence on conformations and dynamics of NTD.

Table 2
Results predicted from the SAAFEC server upon the amino acid change in NTD variants.

	L27A	L28A	V31R
Change in folding free energy (kcal\mol)	−1.33	−2.00	2.76
Difference in vdW (kcal\mol)	−2.59	−3.09	3.56
Difference in electrostatic energy (kt)	0.21	−0.52	12.79
Difference in polar solvation energy (kt)	−0.08	0.09	−11.87
Difference in entropy	−1.46	−1.04	0

3.2. Structural characterization of wild type and mutant NTD

To obtain better insight on the structural dynamics of NTD, we performed MD simulation on the structure of WT NTD and mutants (L27A, L28A and V31R) at 300 K and compared the structural differences observed during the simulation of 250 ns.

To examine the conformational stability of WT NTD and mutants, we calculated Cα-RMSD with respect to the starting structure, as shown in Fig. S1A. The probability distribution plots of RMSD show that the structure of WT is populated around RMSD within the narrow range of 0.15–0.26 nm (Fig. 1A). However, the mutants are populated within the broader range of RMSD of 0.20–0.40 nm (Fig. 1B-D). The higher deviation in RMSD of the mutant as compared to WT suggests that the structure of NTD is destabilized upon mutation. Among the mutants, the structure of L27A is populated around broader RMSD range of 0.25–0.35 nm (Fig. 1B). Remarkably, the RMSD plot of L28A (Fig. 1C) exhibits bimodal distribution representing dissimilarity in the conformational stability compared to that of the WT and other two mutants, L27A and V31R. The broader distribution of RMSD (0.25–0.35 nm) of L28A signify the highly unstable structure. Whereas, V31R is particularly confined to RMSD range 0.25–0.30 nm, indicating less deviation in structure (Fig. 1D). The average RMSD values of different NTD variants are shown in supporting information Table S1.

To determine the structural dynamics of a protein, radius of gyration (R_g) is an effective parameter which defines the relative compactness of the protein structure. The compactness of the conformational structures for the WT and mutant NTD has been illustrated in Fig. S1B. As can be seen, R_g increases in case of mutants. The probability distribution of the R_g values for the WT and mutants are represented in Fig. 2 (A-D). Results show that the distribution of R_g value of WT is confined between 1.54 nm and 1.58 nm, and the native structure is largely populated around R_g ~1.55 nm. Whereas, the population distribution of mutants shows that R_g values are varying between 1.55 nm and 1.65 nm and having higher distribution around ~1.60 nm. As quantified, the average R_g values of L27A, L28A, and V31R are ~1.60 nm, ~1.69 nm, and ~1.62 nm, respectively (Table S1).

These trends thus clearly suggest that the the mutant proteins are less compact than the wild type.

As more compact structures are likely to have higher intramolecular interactions, the results suggested that the mutant NTD structures possess a reduced number of intramolecular interactions and were less stable than the WT NTD.

The fraction of native contacts determines the structural stability of the proteins. The variation of native contacts with respect to time for NTD variants during simulation is shown in Fig. S1 C. Among the three

Table 1
Results predicted from the DynaMut server upon the amino acid change in NTD variants.

Mutations	ΔΔG			$\Delta\Delta S_{vib}$
	DynaMut	ENCoM	DUET	ENCoM
L27A	−1.258 (destabilizing, DS)	−0.422 (DS)	−1.570 (DS)	0.528 (increase in molecular flexibility)
L28A	−1.836 (DS)	−0.886 (DS)	−1.461 (DS)	1.108 (increase)
V31R	−0.911 (DS)	0.008 (neutral)	−1.957 (DS)	−0.010 (decrease)

Table 3
Predictions and confidence scores for the NTD variants obtained from PREDICT-SNP server.

	PredictSNP		MAPP		PhD-SNP		PolyPhen-1		PolyPhen-2		SIFT		SNAP	
	Prediction	Accuracy	Prediction	Confidence score	Prediction	Confidence score	Prediction	Confidence score	Prediction	Confidence score	Prediction	Confidence score	Prediction	Confidence score
L27A	Deleterious	0.75	Deleterious	0.77	Neutra	0.51	Deleterious	0.59	Deleterious	0.54	Deleterious	0.46	Deleterious	0.62
L28A	Deleterious	0.79	Deleterious	0.77	Neutral	0.44	Deleterious	0.59	Deleterious	0.65	Deleterious	0.84	Deleterious	0.85
V31R	Deleterious	0.71	Deleterious	0.88	Neutral	0.55	Deleterious	0.64	Deleterious	0.56	Deleterious	0.79	Deleterious	0.87

mutants, we find large disruption of the native contacts of L28A which again shows the higher destabilizing effect of this mutant on structure stability of NTD. However, the fraction of native contacts in L27A is relatively similar to WT, indicating the presence of folded structure as reported by Mompean et al. [27]. In addition, the shift in the probability distribution of native contacts toward lower values for mutants (Fig. 3 A-D) signifies the loss of native structure which is more dominant in case of L28A mutation (Fig. 3C). Time-dependent change in the solvent accessible surface area (SASA) can be used to monitor the unfolding process for the WT and mutant proteins (Fig. S1D). As can be seen, the SASA of the mutant increases significantly indicating the solvent exposed evolution of non-polar residues involved in the hydrophobic interactions of NTD. The calculation of the average value of SASA of the entire protein showed increasing trends for L27A, V31R, and L28A as compared to WT (Table S1) suggesting the solvation of the hydrophobic core in mutants and thus the presence of unfolded structure.

Furthermore, the probability distribution plot of SASA for the WT and the mutant showed that the mutants have one sharp peak around 96 nm^2, which is considerably greater than the SASA of WT which is confined around 91 nm^2 (Fig. 4 A-D). This moderate increase in the SASA indicates a possible exposure of the hydrophobic core as the structure moves toward unfolded state.

To gain further insight into the flexibility changes resulting from the mutations, we computed the Cα root mean-square fluctuations (RMSF) along the amino acid sequence (Fig. 5). RMSF provides a measure of the flexibility of each backbone Cα atom with respect to its mean position. In case of WT dimeric NTD, the turn I (residues 21–25) and the turn II (residues 45–50) showed highly flexible regions. Moreover, the subunit A of the dimeric NTD has larger fluctuations in the β2-loop region (residues 18–24) whereas the turn II (residues 45–50) exhibited higher fluctuations in subunit B (Fig. 5A). All the three mutations lead to increase in fluctuations of the protein molecule with maximum increase is seen in L28A. In case of mutant NTD, turn I (residues 36–37) and turn II (residues 46–48) displayed increased fluctuations compared to WT. The subunits A and B behave differently in case of L27A (Fig. 5B) and V31R (Fig. 5D) whereas in L28A (Fig. 5C), both the subunits showed similar but maximum fluctuations. In case of L27A, the fluctuations in α-helix (residues 28–36) of subunit A is higher while the residues 21–25 has higher fluctuations in subunit B (Fig. 5B). The turn I (residues 34–38) of subunit A and turn II (residues 46–50) of subunit B has increased fluctuations in case of V31R mutation (Fig. 5D). The enhanced fluctuations of turn regions has been previously reported by our group [26] and the residues Cys39, Gly40 and Asn45 has been associated with the existence of dynamic polarization [19]. Overall, the trend of RMSF is L28A > V31R > L27A > WT.

3.3. Hydrogen bonds

Hydrogen bonds play a crucial role in protein folding and stabilization and is one of the important interactions involved in maintaining the structure of the protein. The time-evolution of H-bonds for the four systems are shown in Supporting information, Fig. S2. Significant loss of intramolecular H-bonds occurs in the first 100 ns in case of L27A and L28A mutations while in V31R the loss of H-bonds occurs only after ~100 ns. The number of H-bonds decreases considerably in the order: L28A > L27A > V31R > WT, indicating the maximum distortion of structure in L28A.

3.4. Protein structure analysis by DSSP

To further understand the effect of mutations in more detail, the time evolution of the secondary structure profiles of NTD variants are shown in Fig. 6. As mentioned earlier, the NTD adopts a compact fold consist of five β -strands and one helix. At 300 K, the overall conformation of WT does not change considerably with only the minor

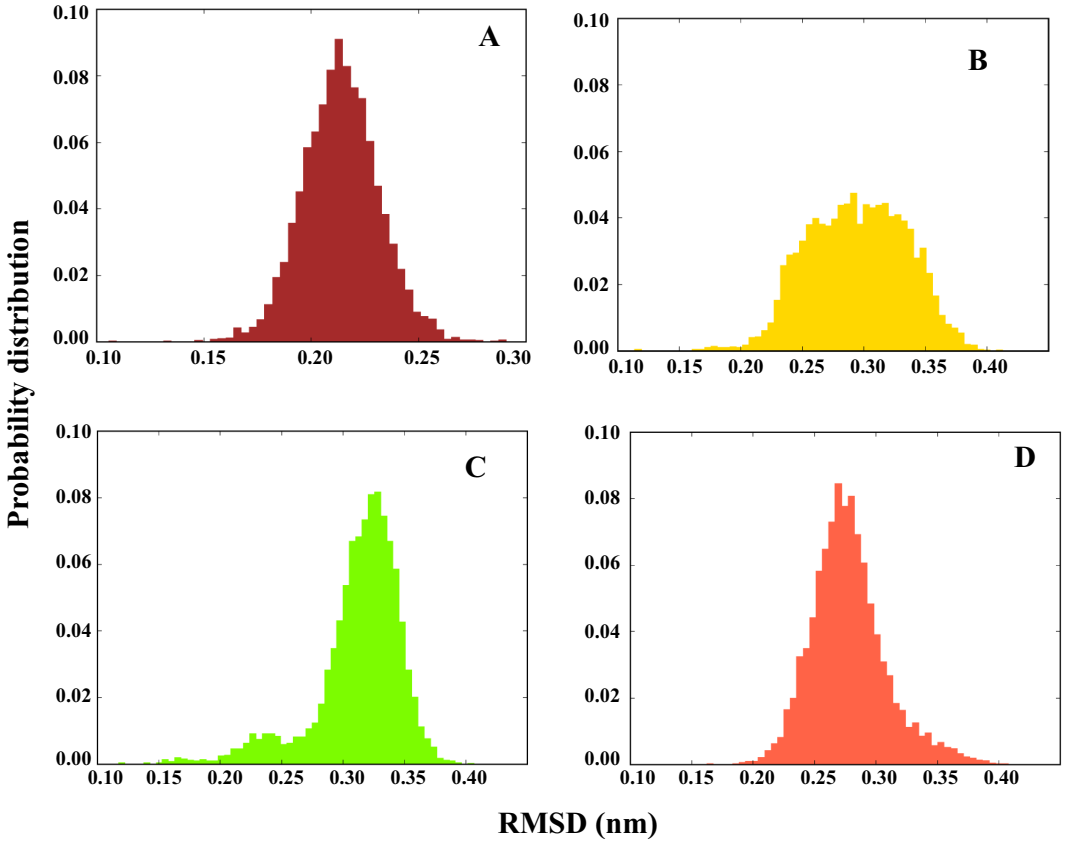

Fig. 1. Probability distributions of structural parameter, C^{α}-RMSD at 300 K for NTD variants. (a) WT, (b) L27A, (c) L28A and (d) V31R.

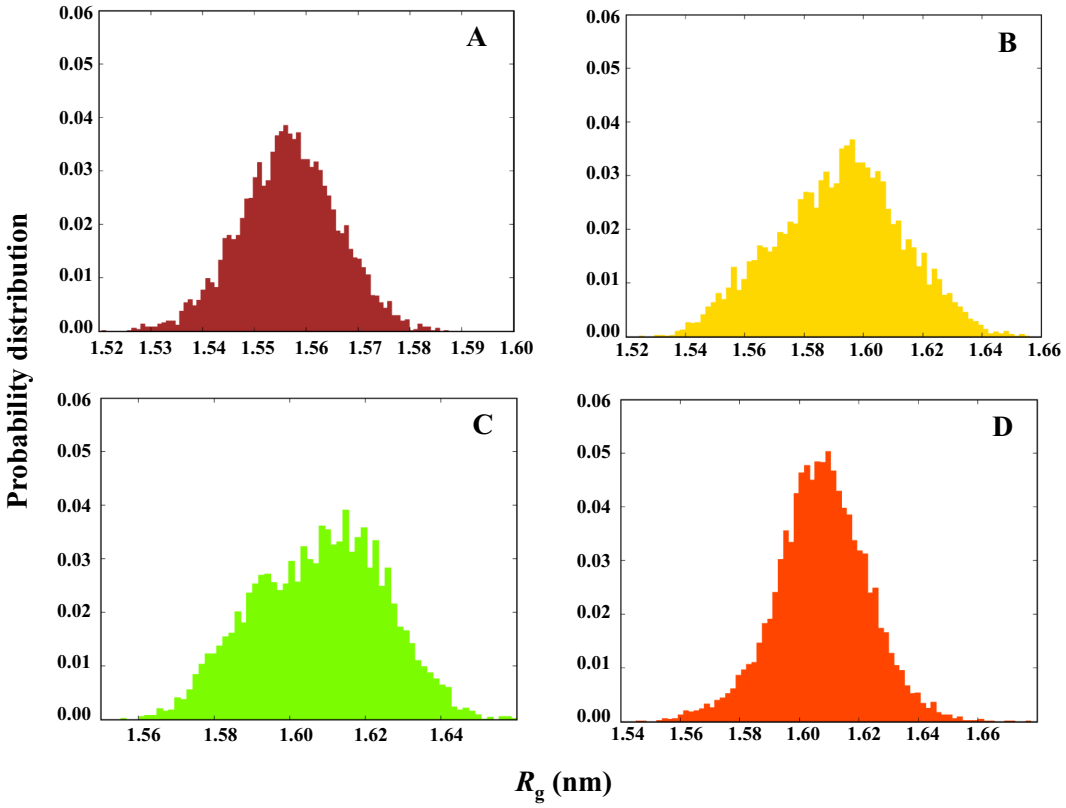

Fig. 2. Probability distributions of R_g at 300 K for (a) WT, (b) L27A, (c) L28A and (d) V31R.

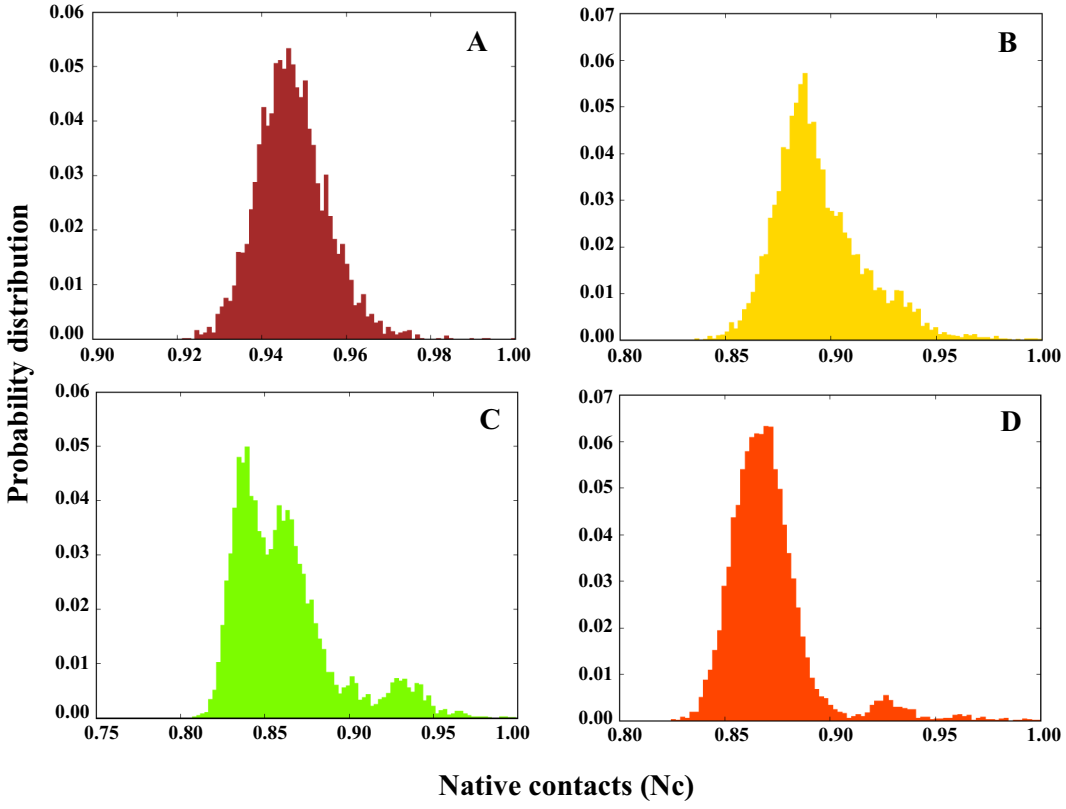

Fig. 3. Probability distributions of native contacts (Nc) at 300 K for (a) WT, (b) L27A, (c) L28A and (d) V31R.

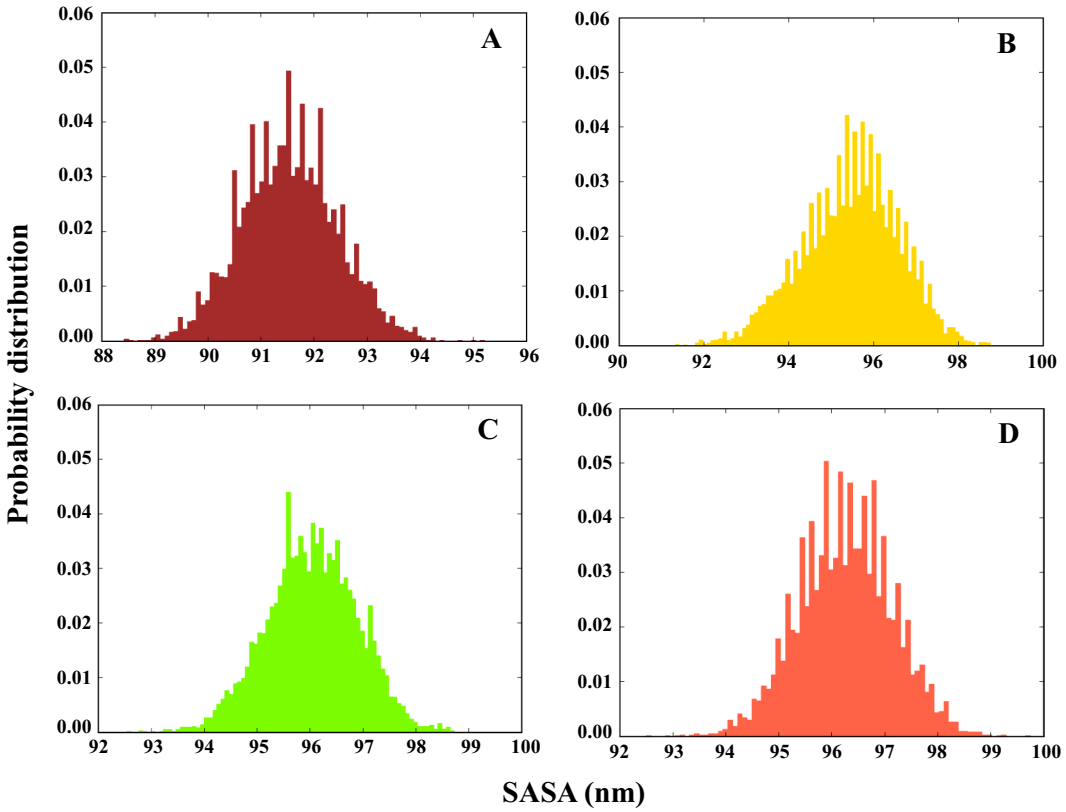

Fig. 4. Probability distributions of SASA at 300 K for (a) WT, (b) L27A, (c) L28A and (d) V31R.

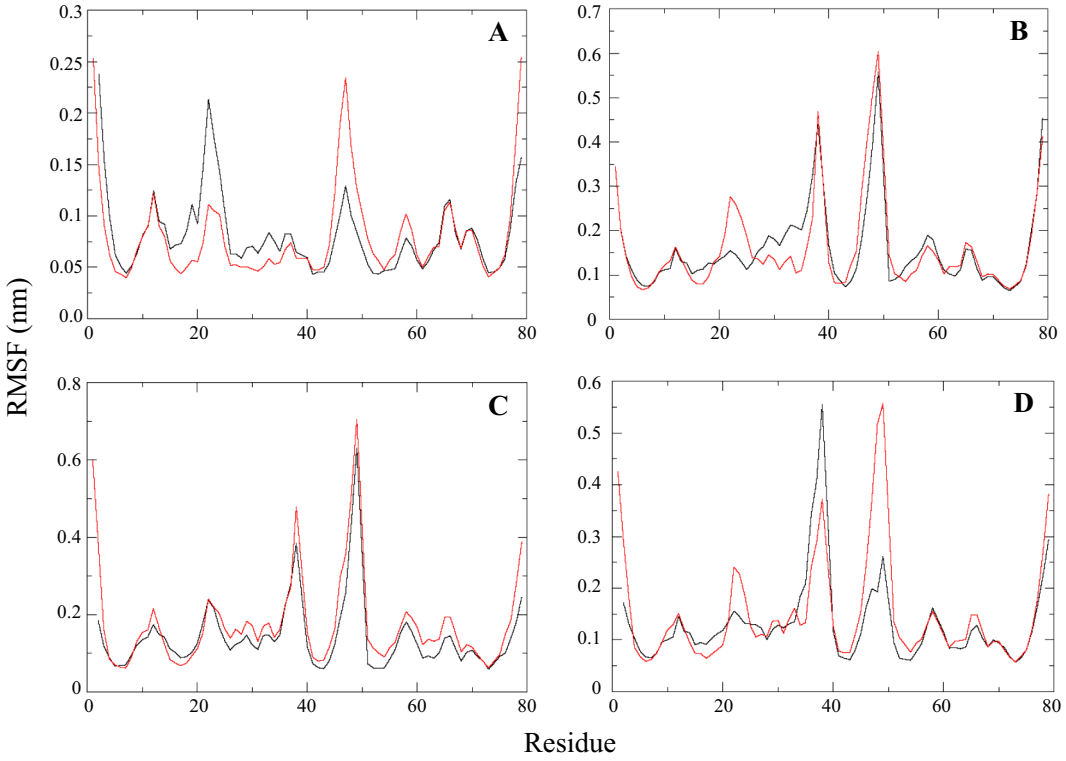

Fig. 5. Positional root-mean-square fluctuations (RMSF) of the backbone C^{α}-atoms for (a) WT, (b) L27A, (c) L28A, and (d) V31R studied in water at 300 K. Black: chain A and Red: chain B of NTD dimer. (For interpretation of the references to color in this figure legend, the reader is referred to the web version of this article.)

extension in β3 (residues 41–45) and β4 (residues 51–53) (Fig. 6A). Notable changes in the secondary structure profile of mutant NTD as compared to WT were observed over 250 ns simulation period (Fig. 6B-D). Most significant changes in all three variants are the loss of turn and bend region near the α1/β3 and β3/β4 region, leading to increase in coil content. The mutant L27A exhibits the largest changes in the secondary structure profile among all three variants (Fig. 6B). In comparison with WT, L27A showed a significant loss of β4 along with minor loss in β3 and β5. The significant loss of strands and irregular secondary structure like turn and bend indicates the destabilization of L27A. Moreover, the subunit B (residues 80–160) remains more stable as compared to subunit A (residues 1–80). Except the loss of turn and bend, we did not observe any significant loss of β-strands in subunit B. We observed a similar loss of both turn and bend to coil in L28A as compared to L27A (Fig. 6C). However, in contrast to L27A, β4 remains stable and the subunit B loses more than subunit A. In the B subunit, β1and β2 strands are lost between 70 ns and 140 ns and then reappear (Fig. 6C). V31R also exhibits the similar pattern of loss of turn and bend regions. However, the α helix of subunit B starts loosening early in the simulation till 200 ns and then regains its helicity. Similarly, the strand β1 and β2 showed substantial loss during ~120 ns to ~160 ns of simulation (Fig. 6D). Overall, change in irregular secondary structures like bend and turn along with concomitant loss of β strands results in a destabilized and unfolded conformation which might leads to dysfunction and aggregation of NTD.

Furthermore, snapshots of the mutant structure obtained at 250 ns of simulation demonstrated the significant loss of secondary structure elements in L27A followed by L28A and V31R (Fig. S3).

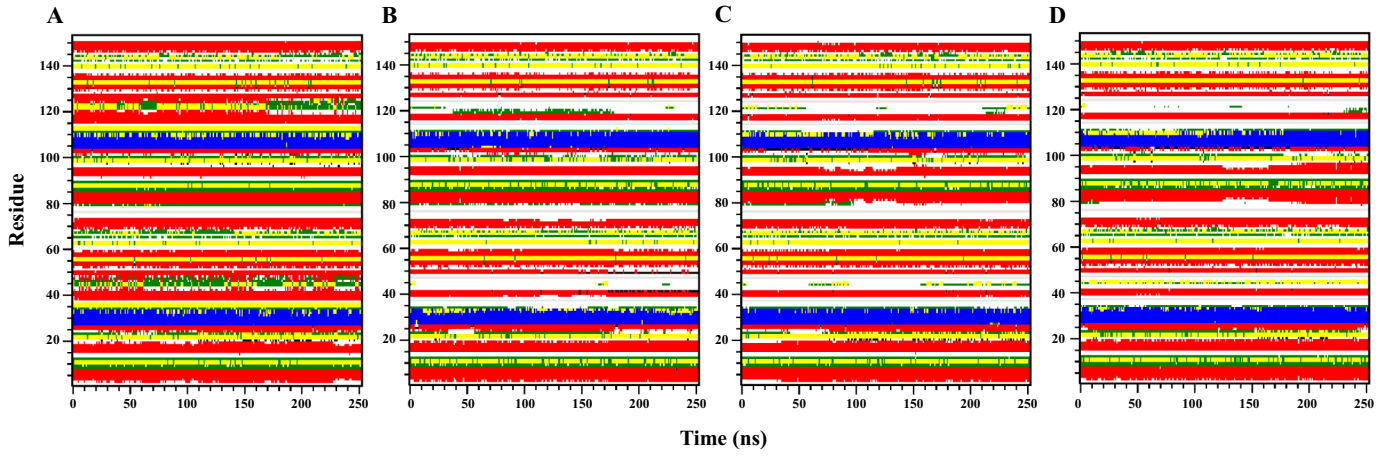

Fig. 6. Secondary structure changes induced by mutation in NTD. Time evolution of the secondary structure profile of (a) WT, (b) L27A, (c) L28A, and (d) V31R during simulations at 300 K. The color codes for the secondary structures are according to the DSSP classification.

3.5. Free energy landscape

The free energy landscape (FEL) provides a quantitative estimate of the relative stability of the WT and mutant NTD structures. All the FELs have been computed by the Boltzmann inversion of the corresponding two-dimensional (2D) probability distribution of the reaction coordinates. In Fig. 7, we compare the FEL with respect to (i) the number of native contacts and (ii) R_g for the WT and three mutants to highlight the mutation induced changes in the conformational stability of different states.

From Fig. 7A, we found that the WT exhibit a stable global minimum restricted within one particular basin indicating the native and folded state of NTD. However, we observed that the mutants had remarkably changed the folding pattern and showed the presence of different metastable states (Fig. 7B-D). The mutation L27A results in larger and disperse basins appeared on the FEL with R_g of 1.56 nm to 1.61 nm and Nc ~ 0.87–0.92, indicating native-like conformations (Fig. 7B). However, FEL of the mutant L28A shows two most favorable basins (Fig. 7C). The first basin (basin I) is located at R_g values varying between 1.60 nm and 1.62 nm with 85%–87% native contacts intact, while the second basin (basin II) is located at R_g values between 1.58 nm and 1.60 nm and 83% of native contacts. The V31R mutation also has a wider basin with R_g values between 1.59 nm and 1.62 nm with ~ 86% - 88% native contacts intact (Fig. 7D).

To probe the sensitivity of ensembles derived from selected reaction coordinates, an additional FEL were calculated as a function of RMSD against Nc (Fig. S4). The overlap between these FEL contour maps depicts excellent agreement and further supports the differences in stability and unfolding of mutants. Therefore, the FEL analysis indicated that the loss in protein stability resulted from a large number of unstable states that indirectly suggest the early unfolding of mutant structures as compared to that of native.

3.6. Essential dynamics

Essential dynamics were employed to investigate the difference in the conformational dynamics of NTD due to mutations. The collective atomic motions of WT NTD and its mutant (L27A, L28A, and V31R) in an essential subspace by projecting the Cα atom shows a cluster representative of explored tertiary conformations along the eigenvectors 1 and 2 (Fig. 8). On comparing the collective motions of the WT and the mutants, we observed clear differences in collective motions due to mutation. The WT displays lesser conformational space with a motional change between −6 and +7 nm in the PC1 axis and −5 to +7 nm in the PC2 axis (Fig. 8A) and exhibits two well-defined clusters. The L27A mutant exhibits three well-defined clusters and larger conformational spaces changes between −6 and +10 nm in the PC1 axis and −8 to +12 nm in the PC2 axis (Fig. 8B). The larger conformational space is observed in the case of L28A, showing motional changes between −10 and +10 nm in the PC1 axis and −8 to +8 nm in the PC2 axis and with three well-defined large clusters (Fig. 8C). The V31R mutant showed two mixed large clusters along with a motion between −8 and +10 nm in the PC1 axis and −9 to +10 nm in the PC2 axis (Fig. 8D). Thus, the ED analysis showed that the mutants explored a larger region of the phase space compared to the WT. The mutations thus increased the collective motions and can destabilize the protein. Moreover, the

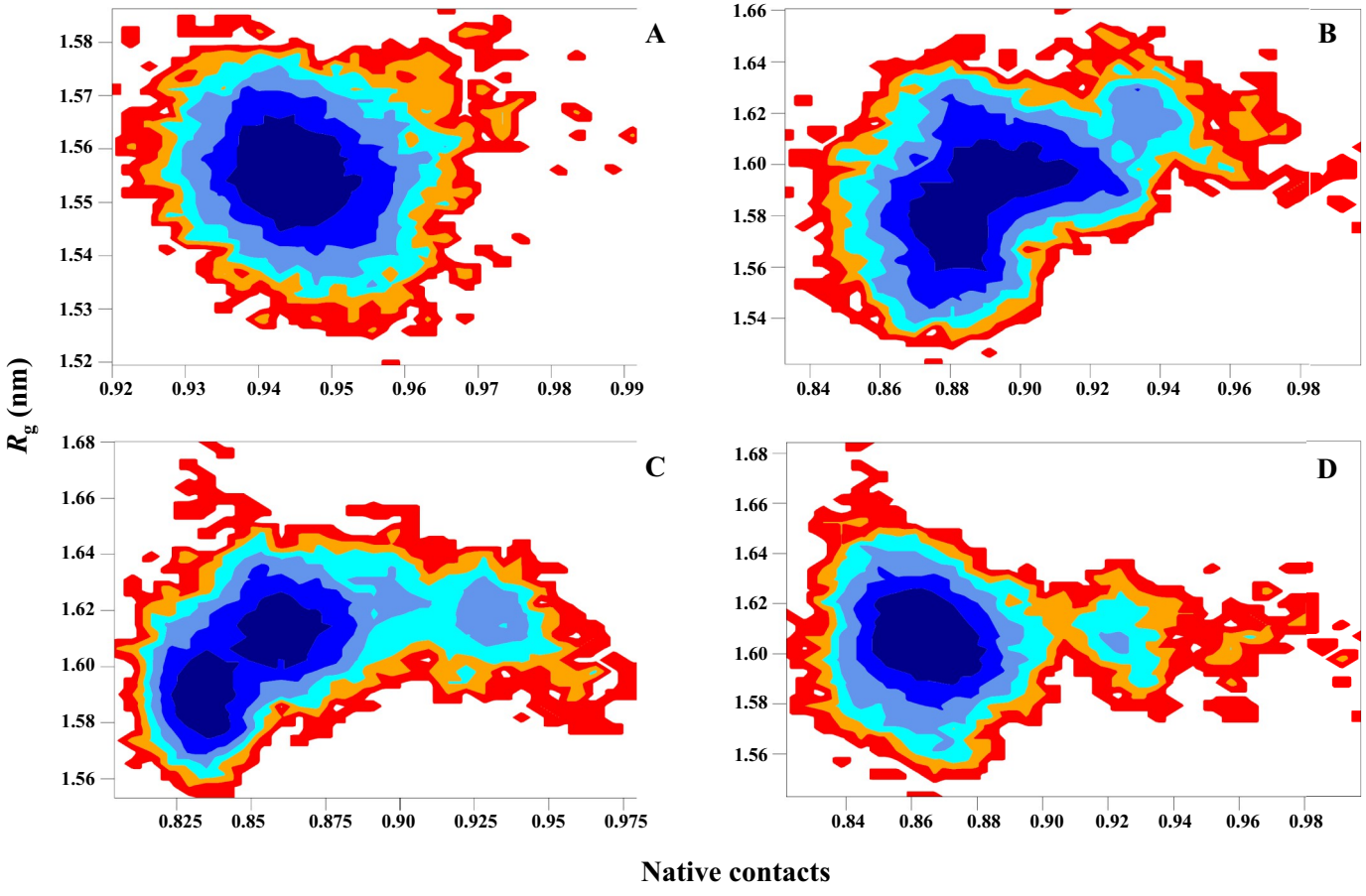

Fig. 7. Free energy contour maps constructed from R_g versus Nc in water for (a) WT, (b) L27A, (c) L28A, and (d) V31R at 300 K. The color is scaled according to kcal/mol.

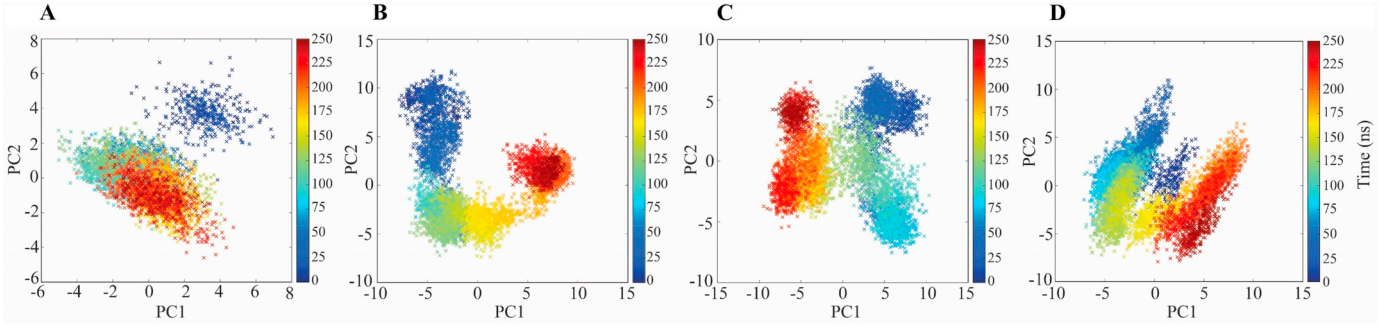

Fig. 8. The conformational landscape sampled by NTD variants. Projection of the motion of the protein in the essential subspace along the eigenvector 1 and 2 for (a) WT, (b) L27A, (c) L28A, and (d) V31R.

change in projection of collective motion could cause impairment in the function of protein [53]. Hence, the increased motion of mutant can prove the dysfunction in mutant NTD observed.

3.7. Loss of interatomic contacts

To better understand the unfolding of the mutant protein, we map the interatomic contacts present in the mutant protein and compare them with WT (Fig. 9). As seen from the figure, a considerable number of the intersubunit contacts are highly separated in both WT (Fig. 9A) and mutant (Fig. 9B–D). The long range interactions involving N-terminal of subunit A and C-terminal of subunit B of the protein were found lost in both the WT and mutants. However, the contact map of L27A is comparable to WT but with some long range contacts absent (Fig. 9B). The loss of long range intersubunit contacts was dominant in case of L28A (Fig. 9C, black circle) and V31R (Fig. 9D). The intrasubunit interactions involving C-terminal residues are also lost in L28A (Fig. 9C, red circle) and V31R (Fig. 9D). Thus, the mutant L28A and V31R represent an unfolded state, with the least number of contacts present in the corresponding map. The weak interstrand and barrel-loop interactions are the results of local unfolding. The local unfolding of strands exposes the hydrophobic core, which makes L28A and V31R

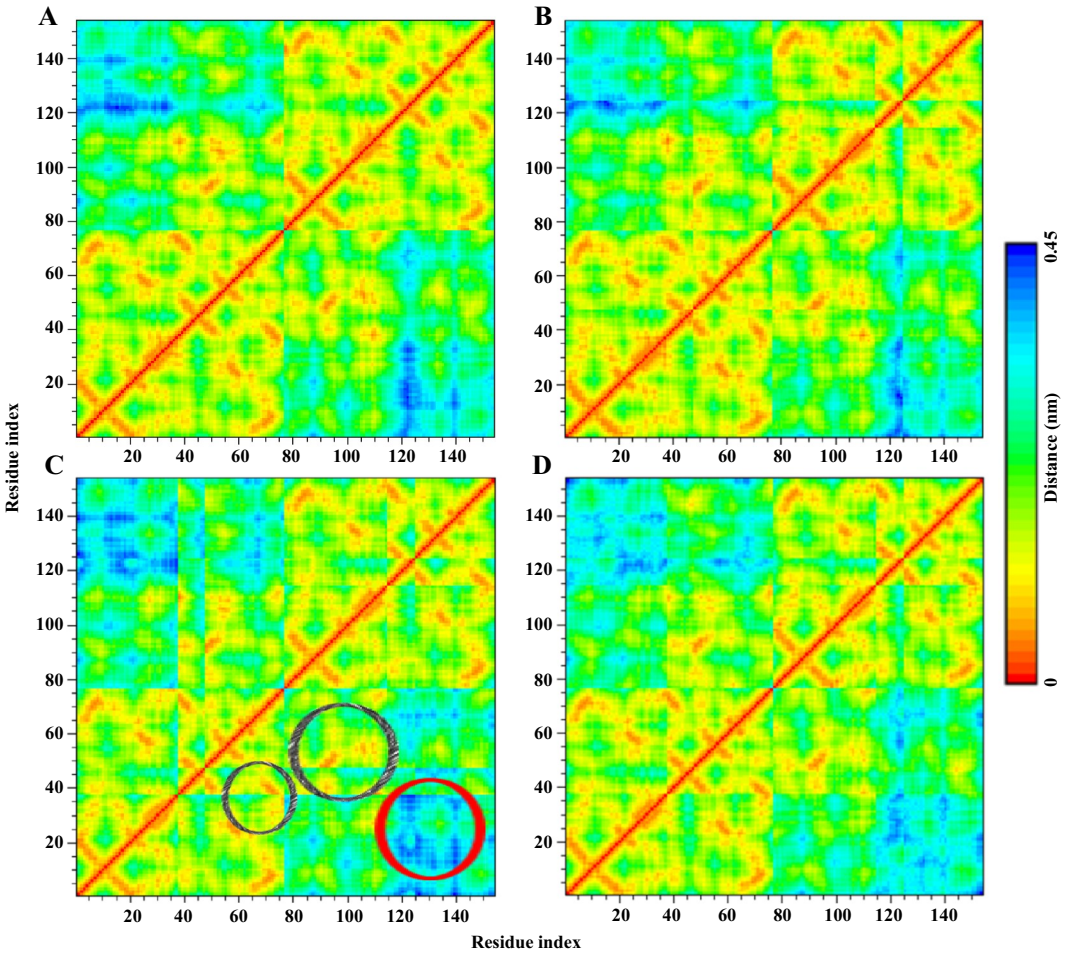

Fig. 9. The local unfolding propensity of the NTD variants. The contact distance map is shown for (a) WT, (b) L27A, (c) L28A, and (d) V31R. The contact between residues i and j is colored in RGB according to the corresponding contact distance.

more prone to aggregation.

3.8. Distance distribution of dimeric interfacial residues

The crystal structure of NTD dimer (PDB ID: 5MDI) [19] showed that the dimeric interface is formed primarily by charge complementation contributed by a positively charged head region [Asn45 (β3), Arg52, Arg55 (β4), Asn76 (β5) and Ser48 (β3-β4 loop)] and a negatively charged tail region [Glu17 (β2), Gln34 (α1-helix) and the Glu14 (β1-β2 loop) and Glu21 (β2-α1loop)]. In addition, at each interface, a parallel inter-molecular β-bridge is formed by H-bonds between Glu17 (β2-strand) with Met51 and Gly53 (β4-strand). This interaction is supported by salt bridges between Arg52- Glu17, and Arg55- Glu21. In addition, Glu17 forms H-bonds with Ser48 and Asn45.

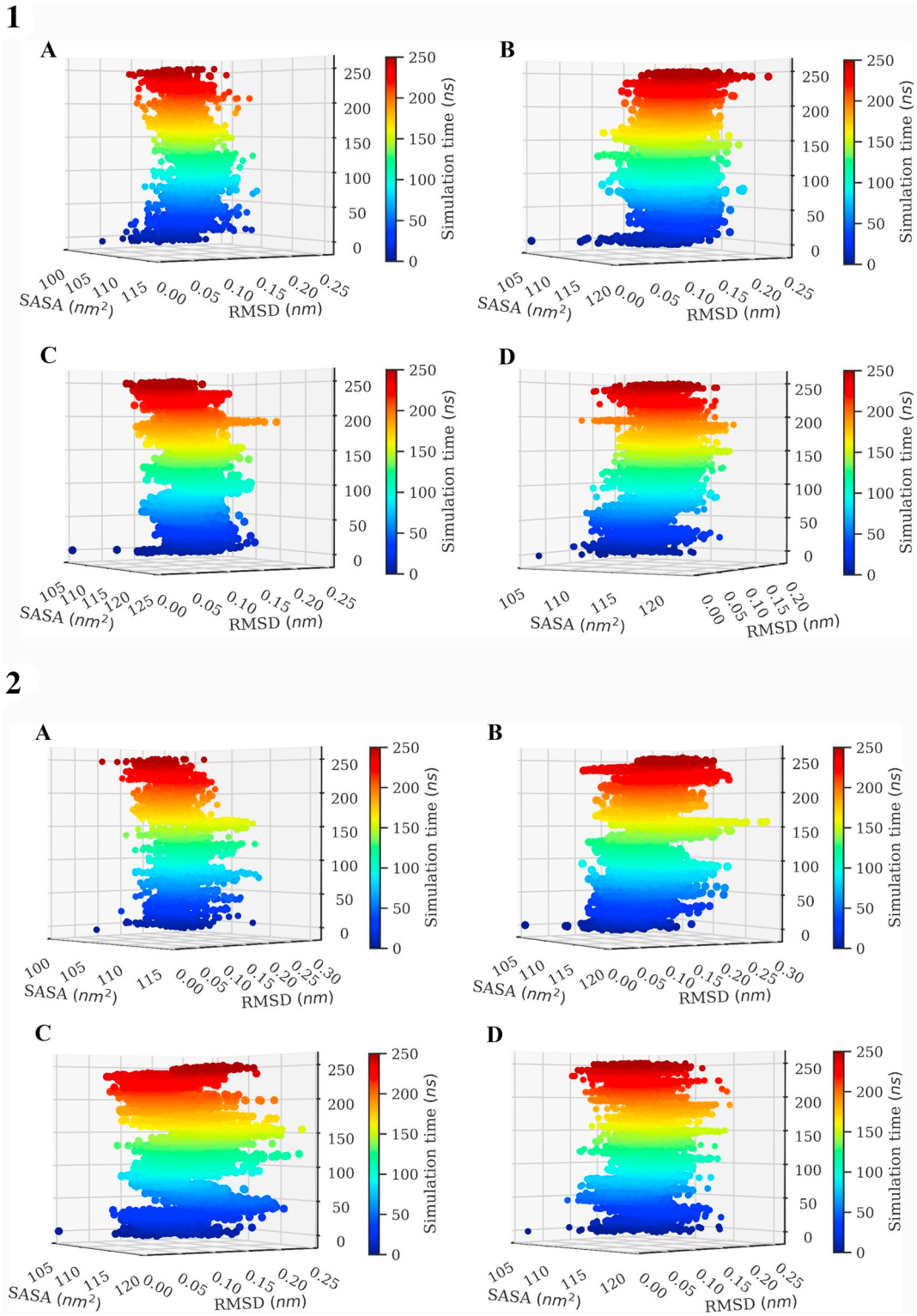

Fig. 10. Time evolution of C^{α}-RMSD and SASA of the side chain of (1) E17, (2) R52, and (3) R55 at 300 K for (a) WT, (b) L27A, (c) L28A, and (d) V31R, respectively. Each point on this plot is colored according to its time of occurrence with the color scale shown.

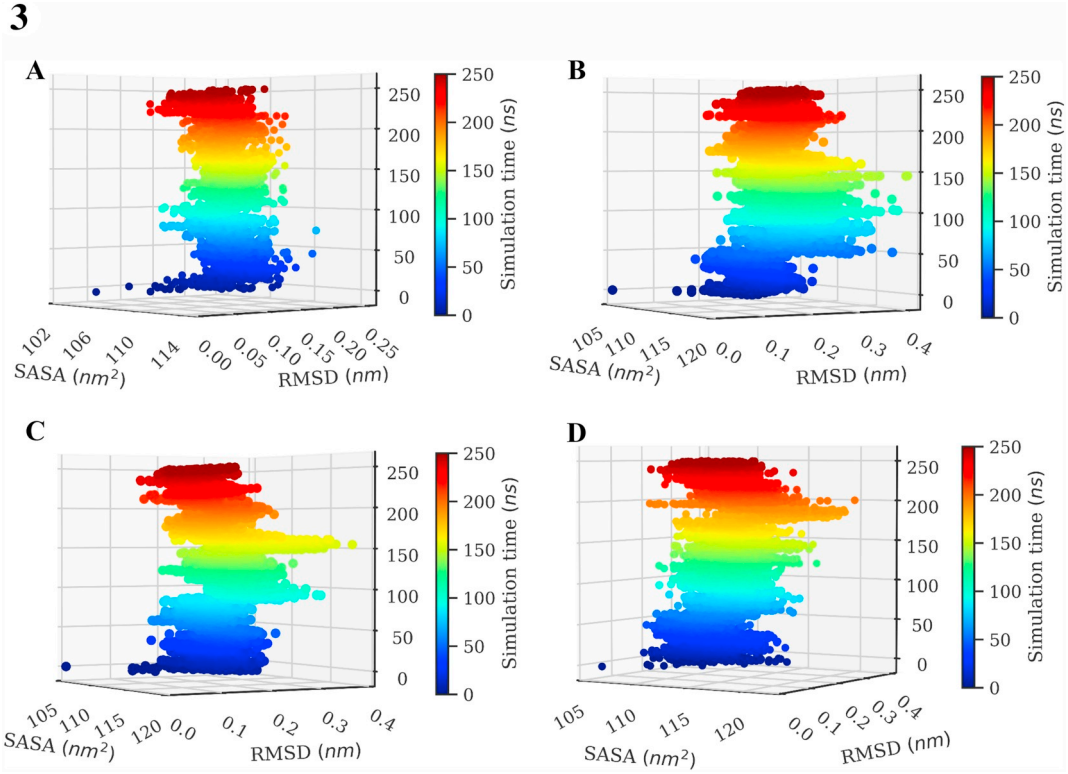

Fig. 10. (*continued*)

Moreover, a small hydrophobic contact at the interface is also formed by the side chains of Ile16 and Pro19 (in subunit B) and Met51, Arg52, and Arg55 (in subunit A). Finally, Gln34 (α1-helix) which makes hydrogen bonds to Leu41 (β3-strand) and Asn76 (β5-strand).

The stability of these hydrogen bonds, salt bridges and hydrophobic contacts may influence the folding, stability and function of the NTD as the disruption of these interactions possibly expose the interface and hydrophobic core of the NTD to the surrounding solvent. To see the effect of mutations on these interactions, we monitored the variations in pairwise distance distributions between some of these contacts and plotted in Fig. S5.

The inter-molecular interactions in all the three mutations were disrupted as indicated by the increase in the pair-wise distance during the simulation. The intermolecular β-bridge between Glu17-Met51 disrupt within 5 ns of simulation in the mutants with the maximum disruption observed in L27A (Fig. S5A). The distance between the H-bond pairs of Glu17-Asn45 (Fig. S5B), and Gln34-Asn76 (Fig. S5C) demonstrated a sharp, significant increase in length within the 5 ns of the simulation suggesting the breaking of these hydrogen bonds.

The salt-bridge between R52 and E17 starts breaking within 5 ns of the simulation with the maximum disruption observed in L27A (Fig. S5D). The disruption of the R55- E21 salt-bridge in L27A occurs only after ~50 ns whereas, in L28A and V31R the loss occurs after ~150 ns and ~175 ns, respectively, indicating the delayed loosening of the interface in case of L28A and V31R (Fig. S5E).

3.9. Time evolution of SASA of interfacial residues

Fig. 10 displays the time evolution of the SASA of the side chain and the Cα-RMSD of interfacial residues E17, R52, and R55 during the simulation of 250 ns in different NTD variants. It shows that in the native fold of NTD, the value of side chain SASA of E17 (Fig. 10A), R52 (Fig. 10B) and R55 (Fig. 10C) ranges from ~100 nm^2 to ~112 nm^2.

In all the three mutations, L27A, L28A, and V31R, these three probes i.e. E17, R52 and R55 becomes mildly buried with a little increase in RMSD, indicating the disruption of NTD interface. The overall change of SASA and RMSD in the probes follows the trend as: V31R > L27A > L28A > WT.

3.10. Distribution of frustration in the protein

Wolynes et al. [54] discussed the concept of frustration to describe the protein folding pathway. The protein folding pathway demonstrates smooth-funneled energy landscape with a small number of energetic conflicts that shows frustration [55–57]. Accordingly, the native contacts should be minimally frustrated, i.e. energetically favorable. In this work, we used the 'Frustratometer' tool [58] to compute and compare the residual frustration in the native and mutant NTD structures. The configurational frustration index of the NTD variants was calculated and we observed that the mutation decreases the percentage of minimally frustrated contacts in NTD (Fig. S6). The results show that among all the native contacts, 24% are minimally frustrated in WT, compared with 22.5%, 22.6% and 21% in L27A, L28A, V31R, respectively. The mutation also decreases the frustration of the substituted residues. The minimally frustrated Leu 27, Leu 28 and Val 31 residues in WT becomes neutral when substituted to Ala or Arg.

The minimally frustrated regions of a protein are required for folding, stability and function [59–62]. The decreased local frustration in mutant NTD could lead to the unfolding, destabilization and dysfunction of NTD. Taken together, these results suggest that NTD mutations, especially V31R decreases the frustration and this could explain the loss of function observed previously.

4. Conclusion

This work intends to shed light on the destabilizing effect of NTD mutations, L27A, L28A and V31R using all-atom MD simulations at 300 K. Various structural parameters like RMSD, Rg, Nc and SASA were analyzed to compare the stability of the four NTD variants. Further the influence of mutations on the residual flexibility, dynamics, free energy

and the motion of NTD were compared. The results indicate that the mutations especially, L28A significantly altered the conformational stability, flexibility and dynamics. The increased propensity of coil formation and loss of β strands upon mutation suggests the reason behind the structural and functional loss of NTD. Subsequently, the intermolecular H-bonds and interfacial interactions were significantly decreased upon mutation. The results form FEL and ED analysis indicates that the folding of NTD was distorted upon mutation. Overall, the results suggested that the mutation possessed toward the structural instability, the reduced intramolecular interactions and the early unfolding of NTD. The results presented in this study are in consistent with experimental studies, and hence provide a better understanding of the relationship between TDP-43 N-terminus and its physiological and pathological roles.

Supplementary data to this article can be found online at https://doi.org/10.1016/j.bpc.2019.106174.

Conflict of interest

The authors declare no conflict of interest.

Acknowledgements

Funding by the Science and Engineering Research Board (SERB), Government of India (Ref. No.: YSS/2015/000228/LS) and DBT Center of Excellence in Bioinformatics (Ref. No.: BT/BI/03/004/2003C) are gratefully acknowledged.

References

[1] M. Neumann, D.M. Sampathu, L.K. Kwong, A.C. Truax, M.C. Micsenyi, T.T. Chou, J. Bruce, T. Schuck, M. Grossman, C.M. Clark, L.F. McCluskey, B.L. Miller, E. Masliah, I.R. Mackenzie, H. Feldman, W. Feiden, H.A. Kretzschmar, J.Q. Trojanowski, V.M. Lee, Ubiquitinated TDP-43 in frontotemporal lobar degeneration and amyotrophic lateral sclerosis, Science 314 (2006) 130–133.

[2] M. Hasegawa, T. Arai, T. Nonaka, F. Kametani, M. Yoshida, Y. Hashizume, T.G. Beach, E. Buratti, F. Baralle, M. Morita, I. Nakano, T. Oda, K. Tsuchiya, H. Akiyama, Phosphorylated TDP-43 in frontotemporal lobar degeneration and amyotrophic lateral sclerosis, Ann. Neurol. 64 (2008) 60–70.

[3] T. Arai, M. Hasegawa, H. Akiyama, K. Ikeda, T. Nonaka, H. Mori, D. Mann, K. Tsuchiya, M. Yoshida, Y. Hashizume, T. Oda, TDP-43 is a component of ubiquitin-positive tau-negative inclusions in frontotemporal lobar degeneration and amyotrophic lateral sclerosis, Biochem. Biophys. Res. Commun. 351 (2006) 602–611.

[4] S. Higashi, E. Iseki, R. Yamamoto, M. Minegishi, H. Hino, K. Fujisawa, T. Togo, O. Katsuse, H. Uchikado, Y. Furukawa, K. Kosaka, H. Arai, Concurrence of TDP-43, tau and alpha-synuclein pathology in brains of Alzheimer's disease and dementia with Lewy bodies, Brain Res. 1184 (2007) 284–294.

[5] H. Nakashima-Yasuda, K. Uryu, J. Robinson, S.X. Xie, H. Hurtig, J.E. Duda, S.E. Arnold, A. Siderowf, M. Grossman, J.B. Leverenz, R. Woltjer, O.L. Lopez, R. Hamilton, D.W. Tsuang, D. Galasko, E. Masliah, J. Kaye, C.M. Clark, T.J. Montine, V.M. Lee, J.Q. Trojanowski, Co-morbidity of TDP-43 proteinopathy in Lewy body related diseases, Acta Neuropathol. 114 (2007) 221–229.

[6] C. Schwab, T. Arai, M. Hasegawa, S. Yu, P.L. McGeer, Colocalization of transactivation-responsive DNA-binding protein 43 and huntingtin in inclusions of Huntington disease, J. Neuropathol. Exp. Neurol. 67 (2008) 1159–1165.

[7] I. Casafont, R. Bengoechea, O. Tapia, M.T. Berciano, M. Lafarga, TDP-43 localizes in mRNA transcription and processing sites in mammalian neurons, J. Struct. Biol. 167 (2009) 235–241.

[8] R.I. Gregory, K.P. Yan, G. Amuthan, T. Chendrimada, B. Doratotaj, N. Cooch, R. Shiekhattar, The microprocessor complex mediates the genesis of microRNAs, Nature 432 (2004) 235–240.

[9] C. Lagier-Tourenne, M. Polymenidou, D.W. Cleveland, TDP-43 and FUS/TLS: emerging roles in RNA processing and neurodegeneration, Hum. Mol. Genet. 19 (2010) R46–R64.

[10] J. Sreedharan, I.P. Blair, V.B. Tripathi, X. Hu, C. Vance, B. Rogelj, S. Ackerley, J.C. Durnall, K.L. Williams, E. Buratti, F. Baralle, J. de Belleroche, J.D. Mitchell, P.N. Leigh, A. Al-Chalabi, C.C. Miller, G. Nicholson, C.E. Shaw, TDP-43 mutations in familial and sporadic amyotrophic lateral sclerosis, Science 319 (2008) 1668–1672.

[11] Y.M. Ayala, T. Misteli, F.E. Baralle, TDP-43 regulates retinoblastoma protein phosphorylation through the repression of cyclin-dependent kinase 6 expression, Proc. Natl. Acad. Sci. U. S. A. 105 (2008) 3785–3789.

[12] C.F. Sephton, S.K. Good, S. Atkin, C.M. Dewey, P. Mayer 3rd, J. Herz, G. Yu, TDP-43 is a developmentally regulated protein essential for early embryonic development, J. Biol. Chem. 285 (2010) 6826–6834.

[13] A. Aulas, C. Vande Velde, Alterations in stress granule dynamics driven by TDP-43 and FUS: a link to pathological inclusions in ALS? Front. Cell. Neurosci. 9 (2015) 423.

[14] S.C. Ling, M. Polymenidou, D.W. Cleveland, Converging mechanisms in ALS and FTD: disrupted RNA and protein homeostasis, Neuron 79 (2013) 416–438.

[15] C.M. Dewey, B. Cenik, C.F. Sephton, D.R. Dries, P. Mayer 3rd, S.K. Good, B.A. Johnson, J. Herz, G. Yu, TDP-43 is directed to stress granules by sorbitol, a novel physiological osmotic and oxidative stressor, Mol. Cell. Biol. 31 (2011) 1098–1108.

[16] C. Colombrita, E. Zennaro, C. Fallini, M. Weber, A. Sommacal, E. Buratti, V. Silani, A. Ratti, TDP-43 is recruited to stress granules in conditions of oxidative insult, J. Neurochem. 111 (2009) 1051–1061.

[17] M. Kato, T.W. Han, S. Xie, K. Shi, X. Du, L.C. Wu, H. Mirzaei, E.J. Goldsmith, J. Longgood, J. Pei, N.V. Grishin, D.E. Frantz, J.W. Schneider, S. Chen, L. Li, M.R. Sawaya, D. Eisenberg, R. Tycko, S.L. McKnight, Cell-free formation of RNA granules: low complexity sequence domains form dynamic fibers within hydrogels, Cell 149 (2012) 753–767.

[18] A. Molliex, J. Temirov, J. Lee, M. Coughlin, A.P. Kanagaraj, H.J. Kim, T. Mittag, J.P. Taylor, Phase separation by low complexity domains promotes stress granule assembly and drives pathological fibrillization, Cell 163 (2015) 123–133.

[19] T. Afroz, E.M. Hock, P. Ernst, C. Foglieni, M. Jambeau, L.A.B. Gilhespy, F. Laferriere, Z. Maniecka, A. Pluckthun, P. Mittl, P. Paganetti, F.H.T. Allain, M. Polymenidou, Functional and dynamic polymerization of the ALS-linked protein TDP-43 antagonizes its pathologic aggregation, Nat. Commun. 8 (2017) 45.

[20] Y.J. Zhang, T. Caulfield, Y.F. Xu, T.F. Gendron, J. Hubbard, C. Stetler, H. Sasaguri, E.C. Whitelaw, S. Cai, W.C. Lee, L. Petrucelli, The dual functions of the extreme N-terminus of TDP-43 in regulating its biological activity and inclusion formation, Hum. Mol. Genet. 22 (2013) 3112–3122.

[21] V. Romano, Z. Quadri, F.E. Baralle, E. Buratti, The structural integrity of TDP-43 N-terminus is required for efficient aggregate entrapment and consequent loss of protein function, Prion 9 (2015) 1–9.

[22] H. Sasaguri, J. Chew, Y.F. Xu, T.F. Gendron, A. Garrett, C.W. Lee, K. Jansen-West, P.O. Bauer, E.A. Perkerson, J. Tong, C. Stetler, Y.J. Zhang, The extreme N-terminus of TDP-43 mediates the cytoplasmic aggregation of TDP-43 and associated toxicity in vivo, Brain Res. 1647 (2016) 57–64.

[23] A. Wang, A.E. Conicella, H.B. Schmidt, E.W. Martin, S.N. Rhoads, A.N. Reeb, A. Nourse, D. Ramirez Montero, V.H. Ryan, R. Rohatgi, F. Shewmaker, M.T. Naik, T. Mittag, Y.M. Ayala, N.L. Fawzi, A single N-terminal phosphomimic disrupts TDP-43 polymerization, phase separation, and RNA splicing, EMBO J. 37 (2018).

[24] C.K. Chang, T.H. Huang, Untangling the structure of the TDP-43 N-terminal domain, FEBS J. 283 (2016) 1239–1241.

[25] P.S. Tsoi, K.J. Choi, P.G. Leonard, A. Sizovs, M.M. Moosa, K.R. MacKenzie, J.C. Ferreon, A.C.M. Ferreon, The N-terminal domain of ALS-linked TDP-43 assembles without Misfolding, Angew. Chem. Int. Ed. Engl. 56 (2017) 12590–12593.

[26] A. Prakash, V. Kumar, N.K. Meena, A.M. Lynn, Elucidation of the structural stability and dynamics of heterogeneous intermediate ensembles in unfolding pathway of the N-terminal domain of TDP-43, RSC Adv. 8 (2018) 19835–19845.

[27] M. Mompean, V. Romano, D. Pantoja-Uceda, C. Stuani, F.E. Baralle, E. Buratti, D.V. Laurents, Point mutations in the N-terminal domain of transactive response DNA-binding protein 43 kDa (TDP-43) compromise its stability, dimerization, and functions, J. Biol. Chem. 292 (2017) 11992–12006.

[28] B.J. Grant, A.P. Rodrigues, K.M. ElSawy, J.A. McCammon, L.S. Caves, Bio3d: an R package for the comparative analysis of protein structures, Bioinformatics 22 (2006) 2695–2696.

[29] V. Frappier, R.J. Najmanovich, A coarse-grained elastic network atom contact model and its use in the simulation of protein dynamics and the prediction of the effect of mutations, PLoS Comput. Biol. 10 (2014) e1003569.

[30] D.E. Pires, D.B. Ascher, T.L. Blundell, mCSM: predicting the effects of mutations in proteins using graph-based signatures, Bioinformatics 30 (2014) 335–342.

[31] A.P. Pandurangan, B. Ochoa-Montano, D.B. Ascher, T.L. Blundell, SDM: a server for predicting effects of mutations on protein stability, Nucleic Acids Res. 45 (2017) W229–W235.

[32] D.E. Pires, D.B. Ascher, T.L. Blundell, DUET: a server for predicting effects of mutations on protein stability using an integrated computational approach, Nucleic Acids Res. 42 (2014) W314–W319.

[33] I. Getov, M. Petukh, E. Alexov, SAAFEC: predicting the effect of single point mutations on protein folding free energy using a knowledge-modified MM/PBSA approach, Int. J. Mol. Sci. 17 (2016) 512.

[34] J. Bendl, J. Stourac, O. Salanda, A. Pavelka, E.D. Wieben, J. Zendulka, J. Brezovsky, J. Damborsky, PredictSNP: robust and accurate consensus classifier for prediction of disease-related mutations, PLoS Comput. Biol. 10 (2014) e1003440.

[35] M.J. Abraham, T. Murtola, R. Schulz, S. Páll, J.C. Smith, B. Hess, E. Lindahl, GROMACS: high performance molecular simulations through multi-level parallelism from laptops to supercomputers, SoftwareX 1-2 (2015) 19–25.

[36] H.J.C. Berendsen, J.R. Grigera, T.P. Straatsma, The missing term in effective pair potentials, J. Phys. Chem. 91 (1987) 6269–6271.

[37] M. Parrinello, A. Rahman, Crystal structure and pair potentials: a molecular-dynamics study, Phys. Rev. Lett. 45 (1980) 1196–1199.

[38] H. Berk, B. Henk, B.J.C. Herman, F.G.E.M. Johannes, LINCS: a linear constraint solver for molecular simulations, J. Comput. Chem. 18 (1997) 1463–1472.

[39] T. Darden, D. York, L. Pedersen, Particle mesh Ewald: an N·log(N) method for Ewald sums in large systems, J. Chem. Phys. 98 (1993) 10089–10092.

[40] A. Prakash, G. Dixit, N.K. Meena, R. Singh, P. Vishwakarma, S. Mishra, A.M. Lynn, Elucidation of stable intermediates in urea-induced unfolding pathway of human carbonic anhydrase IX, J. Biomol. Struct. Dyn. (2017) 1–16.

[41] R.T. McGibbon, K.A. Beauchamp, M.P. Harrigan, C. Klein, J.M. Swails, C.X. Hernandez, C.R. Schwantes, L.P. Wang, T.J. Lane, V.S. Pande, MDTraj: a

modern open library for the analysis of molecular dynamics trajectories, Biophys. J. 109 (2015) 1528–1532.
[43] W. Kabsch, C. Sander, Dictionary of protein secondary structure: pattern recognition of hydrogen-bonded and geometrical features, Biopolymers 22 (1983) 2577–2637.
[44] A. Li, V. Daggett, Characterization of the transition state of protein unfolding by use of molecular dynamics: chymotrypsin inhibitor 2, Proc. Natl. Acad. Sci. U. S. A. 91 (1994) 10430–10434.
[45] V. Kumar, A. Prakash, P. Pandey, A.M. Lynn, M.I. Hassan, TFE-induced local unfolding and fibrillation of SOD1: bridging the experiment and simulation studies, Biochem. J. 475 (2018) 1701–1719.
[46] R.B. Best, G. Hummer, W.A. Eaton, Native contacts determine protein folding mechanisms in atomistic simulations, Proc. Natl. Acad. Sci. U. S. A. 110 (2013) 17874–17879.
[47] A. Prakash, V. Kumar, P. Pandey, D.R. Bharti, P. Vishwakarma, R. Singh, M.I. Hassan, A.M. Lynn, Solvent sensitivity of protein aggregation in Cu, Zn superoxide dismutase: a molecular dynamics simulation study, J. Biomol. Struct. Dyn. (2017) 1–13.
[48] V. Kumar, A. Prakash, A.M. Lynn, Alterations in local stability and dynamics of A4V SOD1 in the presence of trifluoroethanol, Biopolymers 109 (3) (2018 Mar) e23102.
[49] A. Amadei, A.B. Linssen, H.J. Berendsen, Essential dynamics of proteins, Proteins 17 (1993) 412–425.
[50] H. Shukla, R. Shukla, A. Sonkar, T. Pandey, T. Tripathi, Distant Phe345 mutation compromises the stability and activity of Mycobacterium tuberculosis isocitrate lyase by modulating its structural flexibility, Sci. Rep. 7 (2017) 1058.
[51] H. Shukla, R. Shukla, A. Sonkar, T. Tripathi, Alterations in conformational topology and interaction dynamics caused by L418A mutation leads to activity loss of Mycobacterium tuberculosis isocitrate lyase, Biochem. Biophys. Res. Commun. 490 (2017) 276–282.
[52] R. Shukla, H. Shukla, T. Tripathi, Activity loss by H46A mutation in Mycobacterium tuberculosis isocitrate lyase is due to decrease in structural plasticity and collective motions of the active site, Tuberculosis (Edinb) 108 (2018) 143–150.
[53] H.J. Berendsen, S. Hayward, Collective protein dynamics in relation to function, Curr. Opin. Struct. Biol. 10 (2000) 165–169.
[54] D.U. Ferreiro, J.A. Hegler, E.A. Komives, P.G. Wolynes, Localizing frustration in native proteins and protein assemblies, Proc. Natl. Acad. Sci. U. S. A. 104 (2007) 19819–19824.
[55] J.N. Onuchic, Z. Luthey-Schulten, P.G. Wolynes, Theory of protein folding: the energy landscape perspective, Annu. Rev. Phys. Chem. 48 (1997) 545–600.
[56] C. Clementi, S.S. Plotkin, The effects of nonnative interactions on protein folding rates: theory and simulation, Protein Sci. 13 (2004) 1750–1766.
[57] L.L. Chavez, J.N. Onuchic, C. Clementi, Quantifying the roughness on the free energy landscape: entropic bottlenecks and protein folding rates, J. Am. Chem. Soc. 126 (2004) 8426–8432.
[58] R.G. Parra, N.P. Schafer, L.G. Radusky, M.Y. Tsai, A.B. Guzovsky, P.G. Wolynes, D.U. Ferreiro, Protein Frustratometer 2: a tool to localize energetic frustration in protein molecules, now with electrostatics, Nucleic Acids Res. 44 (2016) W356–W360.
[59] D.U. Ferreiro, E.A. Komives, P.G. Wolynes, Frustration in biomolecules, Q. Rev. Biophys. 47 (2014) 285–363.
[60] B. Fuglestad, P.M. Gasper, J.A. McCammon, P.R. Markwick, E.A. Komives, Correlated motions and residual frustration in thrombin, J. Phys. Chem. B 117 (2013) 12857–12863.
[61] S. Gianni, C. Camilloni, R. Giri, A. Toto, D. Bonetti, A. Morrone, P. Sormanni, M. Brunori, M. Vendruscolo, Understanding the frustration arising from the competition between function, misfolding, and aggregation in a globular protein, Proc. Natl. Acad. Sci. U. S. A. 111 (2014) 14141–14146.
[62] S. Husain, V. Kumar, M.I. Hassan, Phosphorylation-induced changes in the energetic frustration in human Tank binding kinase 1, J. Theor. Biol. 449 (2018) 14–22.